High density p-type $Bi_{0.5}Sb_{1.5}Te_3$ nanowires by electrochemical templating through ion-track lithography

Xiaohong Li,[a] Elena Koukharenko,[b] Iris S. Nandhakumar,*[a] John Tudor,[b] Steve P. Beeby[b] and Neil M. White[b]

Received 14th October 2008, Accepted 30th January 2009
First published as an Advance Article on the web 25th February 2009
DOI: 10.1039/b818040g

High density p-type $Bi_{0.5}Sb_{1.5}Te_3$ nanowire arrays are produced by a combination of electrodeposition and ion-track lithography technology. Initially, the electrodeposition of p-type $Bi_{0.5}Sb_{1.5}Te_3$ films is investigated to find out the optimal conditions for the deposition of nanowires. Polyimide-based Kapton foils are chosen as a polymer for ion track irradiation and nanotemplating $Bi_{0.5}Sb_{1.5}Te_3$ nanowires. The obtained nanowires have average diameters of 80 nm and lengths of 20 μm, which are equivalent to the pore size and thickness of Kapton foils. The nanowires exhibit a preferential orientation along the {110} plane with a composition of 11.26 at.% Bi, 26.23 at.% Sb, and 62.51 at.% Te. Temperature dependence studies of the electrical resistance show the semiconducting nature of the nanowires with a negative temperature coefficient of resistance and band gap energy of 0.089 ± 0.006 eV.

1. Introduction

Thermoelectric devices which convert heat into electricity and *vice versa* utilize the Seebeck effect for power generation and the Peltier effect for cooling. The ideal thermoelectric device contains over hundreds of n–p semiconductor couples connected electrically in series and thermally in parallel. Such devices present many advantages, including solid-state operation with no moving parts, long operating lifetime, zero emission, maintenance free and high reliability.[1] Nonetheless, their use has been limited to a rather specific range of applications because of the relatively low energy-conversion efficiency. The efficiency of thermoelectric materials is evaluated in terms of a dimensionless figure of merit ZT, given by $ZT = S^2\sigma T/\kappa$ where S, σ, T and κ are the Seebeck coefficient, electrical conductivity, absolute temperature and thermal conductivity, respectively.[2] In order to enhance the efficiency of thermoelectric energy conversion, a high Seebeck coefficient, an increased electrical conductivity, and a decreased thermal conductivity are required for thermoelectric materials, but these physical properties are often inter-related for bulk systems, making it very difficult to control these variables independently.

Nanostructuring thermoelectric materials has recently emerged as a successful strategy to achieve enhancement in ZT due to quantum confinement effects in nanoscale systems which offers opportunities to vary S, σ, and κ independently.[3–5] Theoretical analysis indicates that the enhancement of ZT in nanostructured systems is mainly due to the increased density of states, but an additional factor is the reduced lattice thermal conductivity resulting from the increased phonon surface scattering in nanostructured system.[6,7] These theoretical predictions have been verified in two-dimensional (2D) PbTe/$Pb_{1-x}Eu_xTe$ quantum-well structures[8] and Bi_2Te_3/Sb_2Te_3 thin film superlattices.[3] Even more exciting are the theoretical predictions for one-dimensional (1D) nanostructured thermoelectric materials,[9,10] which are thought to have remarkable enhancements in ZT compared to 2D systems. These predictions have stimulated research interest in the preparation of 1D nanostructured thermoelectric materials.

Heavily doped Bi_2Te_3 based semiconductors (*e.g.* *n*-type $Bi_2Te_{2.7}Se_{0.3}$ and p-type $Bi_{0.5}Sb_{1.5}Te_3$) are considered to be the most efficient materials for thermoelectric device application because of their superior ZT near room temperature.[1,11] These materials are therefore one of the best targets for the preparation of 1D nanostructures. A variety of approaches have been reported to prepare n-type Bi_2Te_3 1D nanostructures, including templated electrodeposition using anodic alumina,[12–16] surfactant-mediated solvothermal techniques,[17,18] step edge selective electrodeposition,[19] high-temperature organic solution synthesis,[20] low-temperature and template-free synthesis[21] and most recently the galvanic displacement reaction.[22] However, there are only very few reports on the preparation of p-type $Bi_{0.5}Sb_{1.5}Te_3$ 1D nanostructures. Stacy's group made an effort to produce $Bi_{0.5}Sb_{1.5}Te_3$ nanowire arrays by electrodeposition using anodic alumina templates.[23] Due to the insufficiency of the amount of Sb in the electrolyte solution, they applied a negative deposition potential in order to obtain the correct composition of $Bi_{0.5}Sb_{1.5}Te_3$, resulting in rough and dendritic growth and poor wetting of nanowires inside the pores. More recently, Myung's group modified the deposition conditions and obtained $Bi_{0.5}Sb_{1.5}Te_3$ nanowires using commercial polycarbonate membranes as templates.[24,25]

In this paper, we report the preparation of p-type $Bi_{0.5}Sb_{1.5}Te_3$ nanowire arrays by combining electrodeposition with ion-track lithography technology. Ion-track lithography technology is well known as a low-cost process to form deep

[a] *School of Chemistry, University of Southampton, Southampton, UK SO17 1BJ. E-mail: iris@soton.ac.uk; Fax: +44 (0)2380 593781; Tel: +44 (0)2380 594484*
[b] *School of Electronics and Computer Science, University of Southampton, Southampton, UK SO17 1BJ*

 This journal is © the Owner Societies 2009

vertical and high aspect ratio channels for nanowire growth.[26] In considering nanowire growth in templates for thermoelectric applications, the contribution of the host materials must be considered. Here we choose polyimide-based Kapton as a template for electroplating $Bi_{0.5}Sb_{1.5}Te_3$ nanowires. Compared to the anodic alumina templates, Kapton templates have several beneficial properties, *e.g.* high heat resistance, flexural capability, chemical resistance and low dielectric constant.[27] In particular Kapton has a thermal conductivity of 0.14 W m^{-1} K^{-1} which is low enough to be especially interesting for thermoelectric applications.[28] Furthermore, since both electrodeposition and ion-track lithography are compatible with silicon integrated circuit processing, our approach is promising for building MEMS (microelectromechanical system) thermoelectric nanodevices.

2. Experimental

Materials

Bi powder (Alfa Aesar 99.999%), Te powder (Alfa Aesar 99.999%), $SbCl_3$ (Sigma-Aldrich 99$^+$%), $C_6H_8O_7{\cdot}H_2O$ (H_3Cit, Aldrich 99.5%), $Na_3C_6H_5O_7{\cdot}2H_2O$ (Na_3Cit, Sigma-Aldrich 99%), and HNO_3 (Fisher 70%) were all used as received. All aqueous solutions were freshly prepared using reagent grade water (15 MΩ cm^{-1} resistances) from an ELGA water purification system. Polyimide Kapton foils (20 μm thick from Dupont) were irradiated at GSI (Darmstadt, Germany) with Pb^+ ions (kinetic energy 4 MeV u^{-1}, fluence 5×10^9 ions cm^{-2}). The ion-tracked Kapton foils were pre-etched in H_2O_2 (Fisher 30%) solution at 60 °C for 100 min followed by etching in NaClO (Arcros Organics, 13% active chlorine, pH ~ 12.5) solution at 60 °C for 2.5 min. Prior to use as a template for nanowire deposition, one side of the ion-track-etched Kapton foils was coated with a thin layer of evaporated gold and then mounted onto a glass slide substrate using double-sided adhesive copper tape (Agar). The completed substrate was then masked using insulating tape to leave only the unmetallized side of the foil exposed to the electrolyte solution. This was served as a working electrode for nanowire deposition.

Electrodeposition

Electrochemical experiments were carried out in a three-electrode cell using an Autolab potentiostat/galvanostat. A large area platinum gauze and saturated calomel electrode (SCE) served as counter and reference electrodes, respectively. The working electrodes for film deposition were made by evaporating 15 nm chromium onto glass slides followed by 200 nm thick layer of gold. Both films and nanowires were deposited under potentiostatic control at room temperature in unstirred electrolyte solutions containing 0.001 M Bi^{3+}, 0.01 M $HTeO_2^+$, 1 M HNO_3, 0.02M Sb^{3+}, 0.1 M H_3Cit and 0.05 M Na_3Cit. After deposition the Kapton templates were removed either by dissolving them in organic solvent mixtures of *N*-methyl-2-pyrrolidone (NMP, 30 wt%) and monoethanolamine (MEA, 70 wt%) at 100 °C for 1–5 min or by oxygen plasma etching in an Oxford Plasma Technology RIE80plus Etcher at an oxygen pressure of 0.08 T and 300 W at room temperature for 40 min.

Characterization

The surface morphology and compositions of the deposited films and nanowires were characterized using a LEO 1455VP scanning electron microscope (SEM) or JSM-6500F SEM equipped with energy dispersive X-ray (EDX) microanalysis (Oxford Inca 300) and operated at 20 kV. X-Ray diffraction (XRD) data were collected using a Siemens D5000 X-ray diffractometer with Cu Kα radiation (λ = 1.5406 Å). The transport properties of the deposited films were measured using the standard van der Pauw technique with a dc current of 19 mA and a permanent magnetic field of 0.55 T at room temperature on a commercial Hall effect measurement system (HMS 300 from Ecopia). In order to eliminate the influence of the underlying gold substrates on the electrical conductivity measurements, the films were peeled off from the substrates using epoxy resin.[29] The peeled film has an area of 1 × 1 cm. Ohmic contact was made by soldering copper wires with In–Sn solder onto the four corners of the film. An average of ~10 measurements was performed to ensure the reproducibility of the data. The Seebeck coefficient of the film was determined using a custom made Seebeck measurement unit.

The temperature dependence of the electrical resistance of $Bi_{0.5}Sb_{1.5}Te_3$ nanowires was measured using a two-point contact technique. Before each measurement, a thin layer of gold spot was evaporated on the top of the nanowire array to serve as a top contact and a gold seed layer as a bottom contact. Contact to the sample was made using silver paint with gold wires. The sample was mounted in a cryogenic chamber at temperatures ranging from 1.5 to 295 K. *I–V* curves of the nanowires were recorded by a source-meter (Keithley 199) and the resistance R was extracted by using $R = dV/dI$.

3. Results and discussion

3.1 Electrodeposition of p-type $Bi_{0.5}Sb_{1.5}Te_3$ films

In order to ascertain the appropriate deposition conditions for $Bi_{0.5}Sb_{1.5}Te_3$ nanowires, a series of experiments was carried out to examine the effect of deposition conditions on composition, homogeneity, crystallinity and transport properties of the deposited films. The optimal conditions for film deposition are then used as a starting point for the deposition of $Bi_{0.5}Sb_{1.5}Te_3$ nanowires in Kapton templates. Previous studies have shown that electrodeposition of $Bi_{0.5}Sb_{1.5}Te_3$ films is quite challenging due to the fact that it is difficult to achieve sufficient amounts of Sb in the aqueous solution.[23–25,30] In this study, citric acid was chosen as a complexing agent to increase the solubility of Sb in the electrolyte solution because citric acid was found to readily form complexes with Sb[31] and has been used as an efficient agent for extraction of Sb in environmental sample analysis.[32] Fig. 1(a–c) shows the cyclic voltammograms (CV) recorded in various electrolyte solutions containing the individual elements. The deposition of Bi, Te and Sb are occurred at −0.08 V, −0.3 V and −0.4 V *vs*. SCE, respectively. In the CV recorded in the electrolyte solution containing all

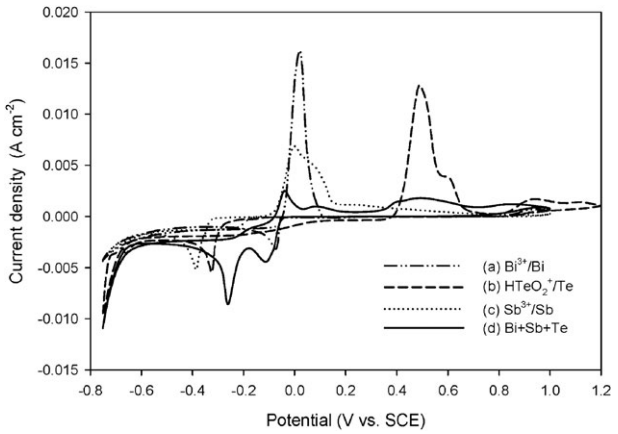

Fig. 1 Cyclic voltammograms of gold working electrodes in various electrolyte solutions containing: (a) 0.001 M Bi^{3+} + 1 M HNO_3; (b) 0.01 M $HTeO_2^+$ + 1 M HNO_3; (c) 0.02 M Sb^{3+} + 0.1 M H_3Cit + 0.05 M Na_3Cit; and (d) 0.001 M Bi^{3+} + 0.01 M $HTeO_2^+$ + 1 M HNO_3 + 0.02 M Sb^{3+} + 0.1 M H_3Cit + 0.05 M Na_3Cit. All voltammograms were recorded at 20 °C at a scan rate of 10 mV s^{-1}.

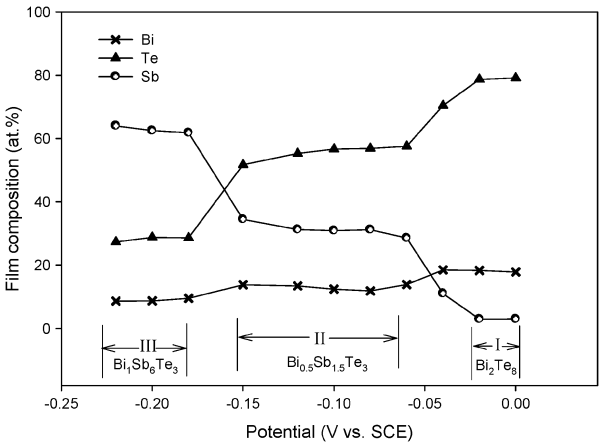

Fig. 2 Film compositions as a function of the applied deposition potentials.

three elements (Fig. 1d) there are only two obvious cathodic peaks observed around −0.09 V and −0.26 V *vs.* SCE, respectively. The first peaks can be attributed to the deposition of Bi and the second one accounts for the co-deposition of Te and Sb, which is shifted towards positive potentials in comparison to those for individual Te and Sb depositions. The behaviour is consistent with previous reports on the deposition of Bi_2Te_3 binary[33] and $Bi_2Te_{3-y}Se_y$ ternary compounds[34] and can be explained by an induced co-deposition mechanism or underpotential deposition mechanism as proposed by Kröger.[35] According to Kröger's analysis, when the two reversible (Nernst) potentials for the two separate elements are closer than ∼0.25 V the deposition of both elements can take place at more positive potentials than those of where either element deposits individually. This process is driven by the free energy associated with the formation of compounds from the elements, in this case, *i.e.* BiSbTe ternary compounds. Based on the CV studies, the potentials for deposition of BiSbTe can be set above the deposition potential of Sb *i.e.* −0.4 V *vs.* SCE, and below the potential where Bi reduction begins, *i.e.*, 0 V *vs.* SCE.

To produce stoichiometric films of $Bi_{0.5}Sb_{1.5}Te_3$ the composition of the deposited films was monitored as a function of the applied deposition potential and determined by EDX. As shown in Fig. 2 for a range of applied potentials, from 0 V to −0.3 V *vs.* SCE there are three distinct regions in which the composition of the films is almost constant whatever the deposition potential is. In the first region of potentials between 0 V and −0.02 V *vs.* SCE the films are composed of almost pure Bi_2Te_8 with only ∼3 at.% Sb, indicating that Sb cannot be easily reduced within this positive potential range. For the second region of potentials between −0.06 V and −0.15 V *vs.* SCE the film composition is approximately ∼10 at.% Bi, ∼30 at.% Sb, and ∼60 at.% Te, close to stoichiometric $Bi_{0.5}Sb_{1.5}Te_3$. As potentials are shifted towards the third region, *i.e.* more negative than −0.18 V *vs.* SCE the film composition changes to $Bi_1Sb_6Te_3$ with a large excess of Sb.

It was found that the deposition potentials also had a significant effect on the surface morphology and crystal structure of the films. Fig. 3 show representative SEM images (a–c) and the corresponding XRD patterns (d–f) for typical films deposited within the different potential regions. The films deposited at −0.02 V (region I) show a granular structure with excellent adhesion on substrates and a prominent {015} crystalline orientation. All of the films with close to stoichiometric composition of $Bi_{0.5}Sb_{1.5}Te_3$ deposited in region II (between −0.06 V and −0.15 V *vs.* SCE) exhibit a cauliflower-like morphology (as typically shown in Fig. 3b) and good adhesion to the substrates and are grey in color. Fig. 3e shows the XRD pattern collected from a particular film which was deposited at −0.08 V *vs.* SCE. According to the standard ICDD PDF card (49–1713), all the detected diffraction peaks can be indexed as those from the rhombohedral $Bi_{0.5}Te_{1.5}Se_3$ ternary crystal [space group (R3m)(166)] except for the gold substrate peaks. This film has a preferential orientation along {110} and {015} planes and the {110} plane is considered to be the optimal crystal orientation for achieving the best thermoelectric performance.[1,23,25] Interpreting the width of the diffraction peaks using the Debye–Sherrer formula gives a grain size of 14 nm. For the films deposited in region III the surface of the films became much rougher and show dendritic growth with poor adhesion to the substrates. The films are black in appearance. The complicated XRD pattern indicates that the resulting film could be a mixture rather than a single phase compound. Taken together, the EDX, SEM and XRD results indicate that the appropriate potential for producing $Bi_{0.5}Sb_{1.5}Te_3$ films should be around −0.08 V *vs.* SCE at which the deposited films have closest stoichiometric composition and the ideal crystalline orientation for thermoelectric performance.

The transport properties (*i.e.* electrical resistivity, carrier concentration, and Hall mobility) of the $Bi_{0.5}Sb_{1.5}Te_3$ film deposited at −0.08 V *vs.* SCE were measured at room temperature using a Hall measurement system. The thickness of the film was 10 μm as observed using SEM. Hall measurement showed that the film was a p-type semiconductor, which was evident by the positive sign of the Hall voltage. The electrical resistivity of the film was about 0.13 Ω cm as determined using

 This journal is © the Owner Societies 2009

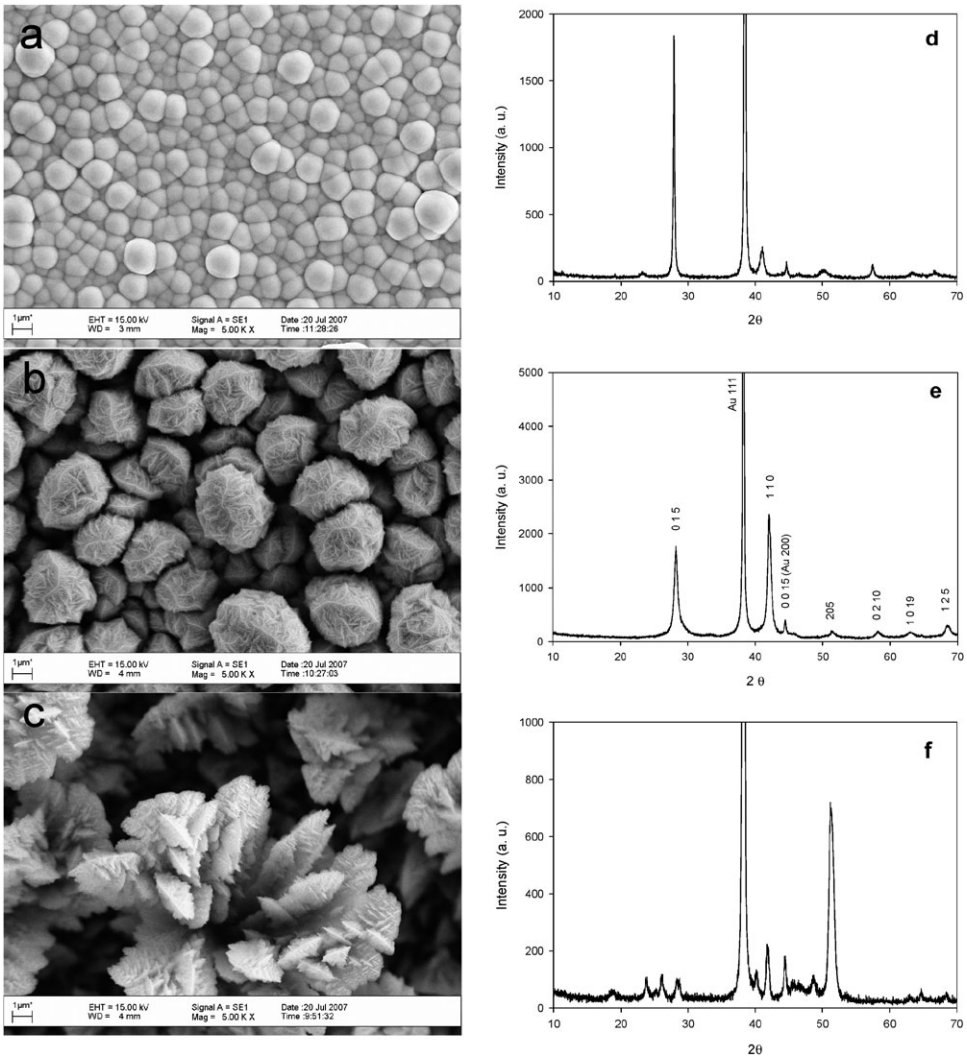

Fig. 3 Representative SEM images (a–c) and corresponding XRD patterns (d–f) for typical films deposited at different potential regions.

the van der Pauw technique. The carrier concentration, Hall mobility and Hall coefficient of the film was found to be 4.7×10^{18} cm^{-3}, 10.8 cm^2 V^{-1} s^{-1}, and 1.5 cm^3 C^{-1}, respectively. The measured Seebeck coefficient of the film was 122 μV K^{-1} at room temperature. The positive value confirmed that the film is p-type, which is in good agreement with the Hall measurement.

3.2 Electrodeposition of p-type $Bi_{0.5}Sb_{1.5}Te_3$ nanowires

Based on the above studies for film deposition, stoichimetric p-type $Bi_{0.5}Sb_{1.5}Te_3$ nanowires can be deposited at a potential of −0.08 V *vs.* SCE using ion-track etched Kapton foils. Fig. 4 shows the SEM image of the etched Kapton foil. The pores are round in shape with an average pore diameter of ~80 nm. The pore diameter is monitored by etching conditions such as etching time, temperature and pH of etching solution.[36] By carefully controlling these conditions, polyimide-based templates with pore diameters below 20 nm have been achieved.[37] This demonstrates the possibility of further reducing the nanowire diameter and achieving a high aspect ratio to enhance the thermoelectric properties. The Kapton foil became uniformly dark-grey in color during deposition, indicating that the pores were etched through the whole foil and resulted in the smooth deposition of nanowires inside the pores.

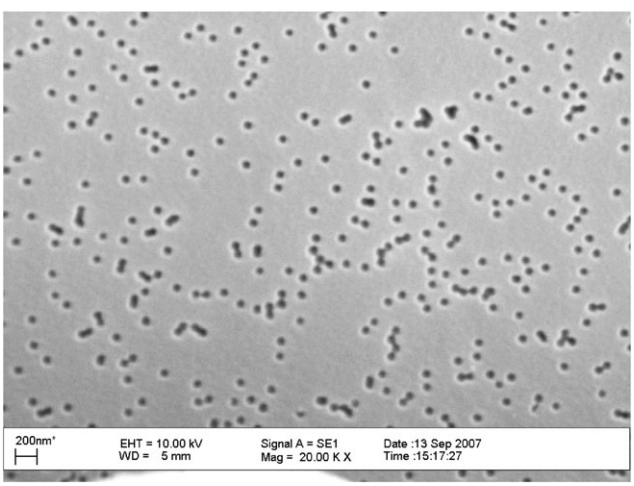

Fig. 4 SEM image of ion-track etched Kapton foils.

Nanowire growth was monitored by a current–time transient curve and stopped when a rapid increase in current was observed, which indicated that some of the pores were filled and the overgrowth of the nanowires occurred across the top surface. Cross sectional SEM image (Fig. 5a) show that the wires were continuous and dense with ~80 nm in diameter and ~20 μm in length, which were the same as the pore size and thickness of the Kapton foil used. EDX analysis revealed the composition of the nanowires to be 11.26 at.% Bi, 26.23 at.% Sb, and 62.51 at.% Te.

After electrodeposition, the Kapton foils can be removed either by dissolution in organic solvent mixtures of NMP/MEA or by oxygen plasma etching. When dissolved in organic solvent mixtures at 100 °C for 1 min, as shown in Fig. 5b the foil was partially removed and the nanowires retained within the foil as bundles. After dissolving for 5 min the nanowires were thoroughly liberated from the foils (Fig. 5c). The obtained wires have an average diameter of 80 nm which is equivalent to the pore size of the Kapton foils. In the case using oxygen plasma for etching, it can be seen from Fig. 5d that freestanding nanowires in the form of highly-ordered arrays can be obtained. An XRD pattern of the nanowires embedded in Kapton foils is shown in Fig. 6. Except for the gold peak that originates from the evaporated seed layer only the {110} peak of the $Bi_{0.5}Sb_{1.5}Te_3$ can be seen clearly. It indicates that the preferred growth direction for the nanowires is along the {110} plane.

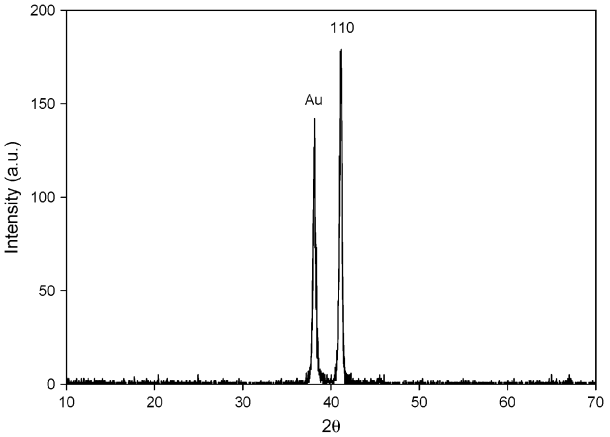

Fig. 6 XRD pattern for $Bi_{0.5}Sb_{1.5}Te_3$ nanowires embedded in Kapton foil. The peak around 38° can be attributed to gold that was used as a seed layer for electrodeposition.

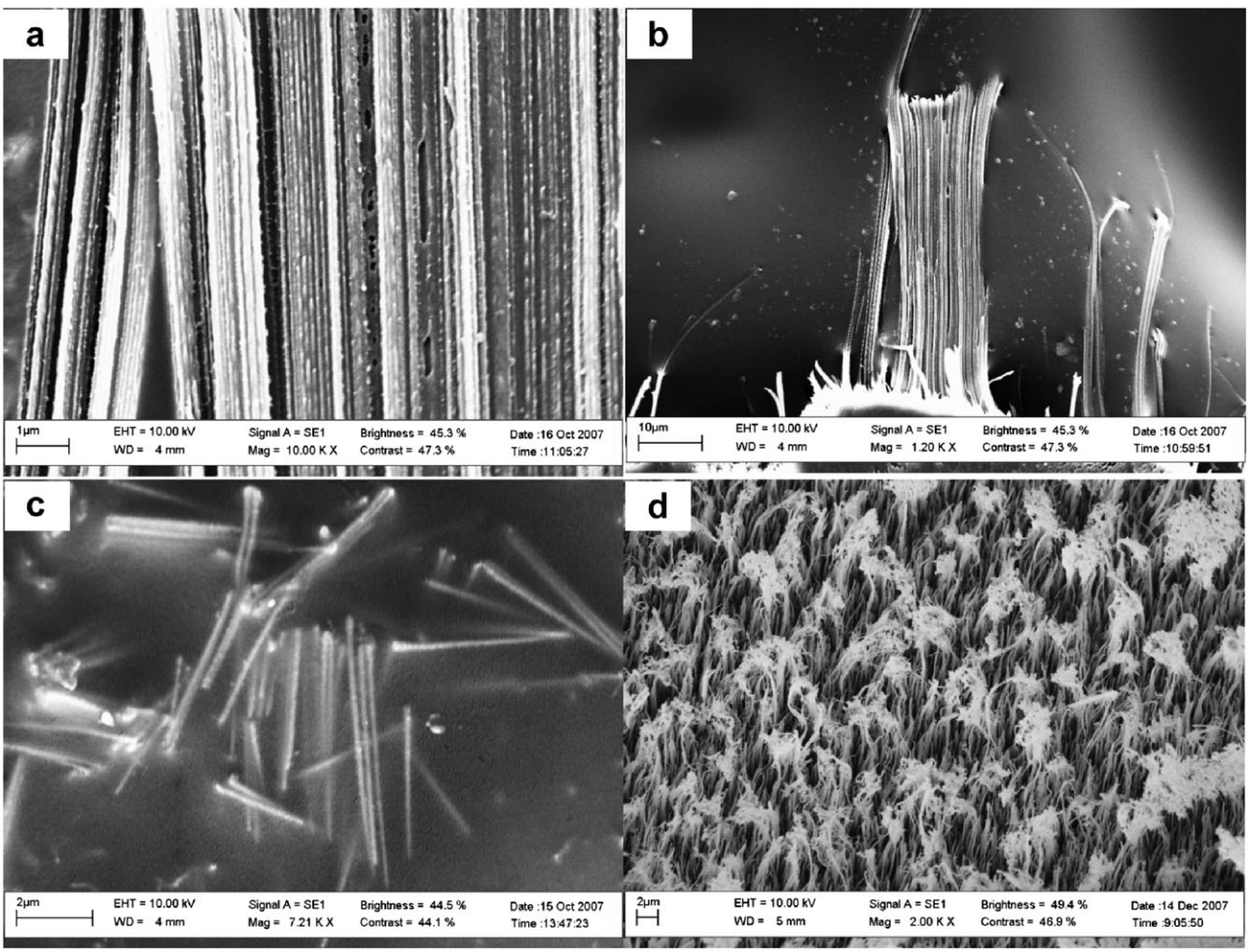

Fig. 5 SEM images of $Bi_{0.5}Sb_{1.5}Te_3$ nanowires embedded in Kapton foil (a), and liberated from Kapton foil by dissolving in organic solvent of NMP/MEA at 100 °C for 1 min (b), and 5 min (c), or by oxygen plasma etching at 0.08 T and 300 W for 40 min (d).

 This journal is © the Owner Societies 2009

3.3 Electrical transport properties of p-type $Bi_{0.5}Sb_{1.5}Te_3$ nanowires

From 1.5–295 K all the *I–V* curves obtained from the $Bi_{0.5}Sb_{1.5}Te_3$ nanowires show linear behavior, confirming good Ohmic contact to the nanowires. Fig. 7(a) shows the temperature dependence of the resistance of the nanowire array (solid line), $R(T)$, normalized to the resistance at 295 K, R_0. It can be observed that the resistance of the nanowires decreases with increasing temperature, which indicates the semiconducting nature of the nanowires. The measured resistance as a function of temperature changes from a linear-like temperature dependence ($T > 50$ K) to an exponential-like dependence ($T < 50$ K) as the temperature decreases. This feature is quite different from that observed on the $Bi_{0.5}Sb_{1.5}Te_3$ film in which the resistance decreases with increasing temperature at all temperature range from 1.5–295 K (dash line) and can be explained in terms of the relative importance of carrier-phonon scattering and carrier-boundary scattering.[38] At high temperature ($T > 50$ K), the phonon scattering dominates and the resistance rises with decreasing temperature. As the temperature decreases below 50 K, the boundary scattering becomes more and more important and dominates the scattering mechanism. Since the nanowires studied in the present work are polycrystalline with potentially many grain boundaries, the contribution of scattering from wire walls together with the grain boundaries may give rise to a more temperature dependent resistance. Therefore, the resistance at low temperature exhibits more temperature variation than that at high temperature. Further analysis shows that the nanowires have a negative temperature coefficient of resistance, which decreased to -0.09 K^{-1} with decreasing temperature from 295 to 1.5 K.

By applying an equation that reflects the temperature dependence of the intrinsic carrier density in a semiconductor: $R(T) = R_0\exp(E_g/2k_BT)$, [39,40] the energy band gap E_g (or thermal activation energy E_a[25]), can be determined. The fit of the high temperature data for the nanowire array and film can be calculated from Fig. 7(b) according to the equation. The value of E_g (E_a) for the nanowires was found to be 0.089 ± 0.006 eV, which is higher than that of the film, 0.045 ± 0.011 eV. This increased band gap may be due to size effects or carrier localization.[25] Currently, further investigations are being undertaken to prepare p-type $Bi_{0.5}Sb_{1.5}Te_3$ nanowires with various diameters down to 20 nm to confirm the above experimental result and to observe some quantum confinement effects.

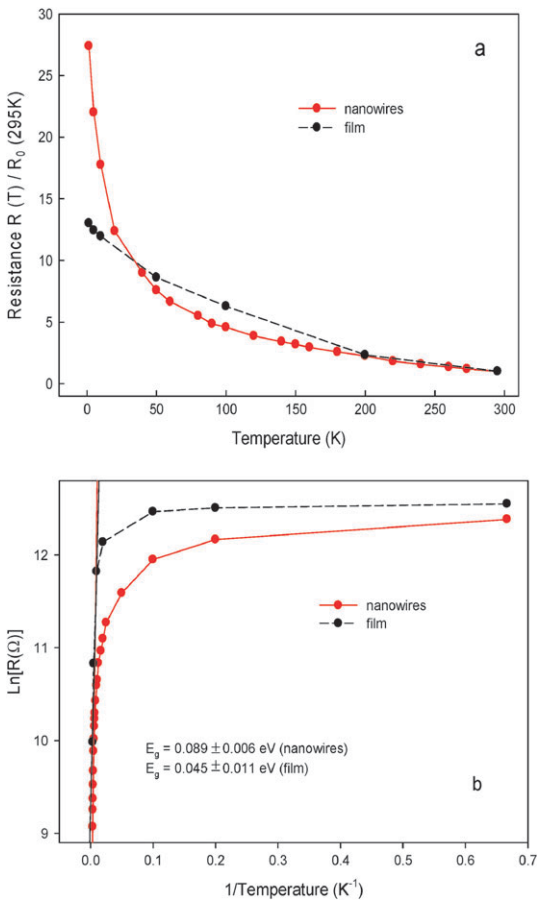

Fig. 7 Temperature dependence of the electrical resistance (a) and the determination of energy band gap (b) of $Bi_{0.5}Sb_{1.5}Te_3$ nanowire array (solid line) and film (dash line).

4. Conclusions

High density p-type $Bi_{0.5}Sb_{1.5}Te_3$ nanowire arrays have been produced by combining electrodeposition with ion-track lithography technology. The electrodeposition conditions have significant effects on composition, homogeneity, crystallinity and transport properties of the deposited materials. It is found that the stoichiometric $Bi_{0.5}Sb_{1.5}Te_3$ nanowires can be obtained at deposition potential of -0.08 V *vs.* SCE. Polyimide-based Kapton foils are good candidate for ion track irradiation and nanotemplating the $Bi_{0.5}Sb_{1.5}Te_3$ nanowires. The obtained nanowires have average diameters of 80 nm and lengths of 20 μm which are equivalent to the pore size and thickness of the Kapton foils. The nanowires exhibit a preferential orientation along the {110} plane and a stoichiometric composition of 11.26 at.% Bi, 26.23 at.% Sb, and 62.51 at.% Te. The study of the temperature dependence of the electrical resistance indicates that the nanowires are semiconducting with a band gap energy of 0.089 ± 0.006 eV, which is higher than that of the film, 0.045 ± 0.011 eV.

Acknowledgements

This work is supported by the Engineering and Physical Science Research Council (EPSRC, grant code EP/D076250). We thank Dr Kanad Mallik, Mr Kevin Martin, and Prof. Peter de Groot for useful help and discussions regarding the transport property measurement, Mr. Jonathan D. Speed for the development of the nanotemplate etching, and GSI for the ion-track irradiation.

References

1 D. M. Rowe, *Handbook of Thermoelectrics*, CRC, Boca Raton, 1995.
2 H. J. Goldsmid, *Thermoelectric Refrigeration*, Plenum, New York, 1964.

3 R. Venkatasubramanian, E. Siivola, T. Colpitts and B. O'Quinn, *Nature*, 2001, **413**, 597.
4 T. C. Harman, P. J. Taylor, M. P. Walsh and B. E. LaForge, *Science*, 2002, **297**, 2229.
5 G. Chen, M. S. Dresselhaus, G. Dresselhaus, J. P. Fleurial and T. Caillat, *Int. Mater. Rev.*, 2003, **48**, 45.
6 L. D. Hicks and M. S. Dresselhaus, *Phys. Rev. B: Condens. Matter Mater. Phys.*, 1993, **47**, 12727.
7 L. D. Hicks and M. S. Dresselhaus, *Phys. Rev. B: Condens. Matter Mater. Phys.*, 1993, **47**, 16631.
8 L. D. Hicks, T. C. Harman, X. Sun and M. S. Dresselhaus, *Phys. Rev. B*, 1996, **53**, 10493.
9 M. S. Dresselhaus, G. Dresselhaus, X. Sun, S. B. Cronin and T. Koga, *Phys. Solid State*, 1999, **41**, 679.
10 X. Sun, Z. Zhang and M. S. Dresselhaus, *Appl. Phys. Lett.*, 1999, **74**, 4005.
11 G. S. Nolas, J. Sharp and H. J. Goldsmid, *Thermoelectrics Basic Principles and New Materials Developments*, Springer, New York, 2001.
12 S. A. Sapp, B. B. Lakshmi and C. R. Martin, *Adv. Mater.*, 1999, **11**, 402.
13 A. L. Prieto, M. S. Sander, M. S. Martín-González, R. Gronsky, T. Sands and A. M. Stacy, *J. Am. Chem. Soc.*, 2001, **123**, 7160.
14 M. S. Sander, A. L. Prieto, R. Gronsky, T. Sands and A. M. Stacy, *Adv. Mater.*, 2002, **14**, 665.
15 C. Jin, X. Xiang, C. Jia, W. Liu, W. Cai, L. Yao and X. Li, *J. Phys. Chem. B*, 2004, **108**, 1844.
16 L. Li, Y. Yang, X. Huang, G. Li and L. Zhang, *Nanotechnology*, 2006, **17**, 1706.
17 H. Yu, P. C. Gibbons and W. E. Buhro, *J. Mater. Chem.*, 2004, **14**, 595.
18 Y. Deng, C. Cui, N. Zhang, T. Ji, Q. Yand and L. Guo, *Solid State Commun.*, 2006, **138**, 111.
19 E. J. Menke, Q. Li and R. M. Penner, *Nano Lett.*, 2004, **4**, 2009.
20 W. Lu, Y. Ding, Y. Chen, Z. L. Wang and J. Fang, *J. Am. Chem. Soc.*, 2005, **127**, 10112.
21 A. Purkayastha, F. Lupo, S. Kim, T. Borca-Tasciuc and G. Ramanath, *Adv. Mater.*, 2006, **18**, 496.
22 F. Xiao, B. Yoo, K. H. Lee and N. V. Myung, *J. Am. Chem. Soc.*, 2007, **129**, 10068.
23 M. M. Gonzalez, A. L. Prieto, R. Gronsky, T. Sands and A. M. Stacy, *Adv. Mater.*, 2003, **15**, 1003.
24 B. Yoo, F. Xiao, K. N. Bozhilov, J. Herman, M. A. Ryan and N. V. Myung, *Adv. Mater.*, 2007, **19**, 296.
25 F. Xiao, B. Yoo, K. H. Lee and N. V. Myung, *Nanotechnology*, 2007, **18**, 335203.
26 C. R. Martin, *Science*, 1994, **266**, 1961.
27 M. Lindeberg and K. Hjort, *Microsyst. Technol.*, 2004, **10**, 608.
28 C. S. Subramanian, T. Amer, B. T. UpChurch, D. W. Alderfer, C. Burkett and B. Sealey, *ISA Trans.*, 2006, **45**, 313.
29 M. Takahashi, M. Kojima, S. Sato, N. Ohnisi, A. Nishiwaki, K. Wakita, T. Miyuki, S. Ikeda and Y. Muramatsu, *J. Appl. Phys.*, 2004, **96**, 5582.
30 D. D. Frari, S. Diliberto, N. Stein, C. Boulanger and J. M. Lecuire, *Thin Solid Films*, 2005, **483**, 44.
31 J. Zheng, A. Iijima and N. Furuta, *J. Anal. At. Spectrom.*, 2001, **16**, 812.
32 R. Miravet, E. Bonilla, J. F. Ló pez-Sánchez and R. Rubio, *J. Environ. Monit.*, 2005, **7**, 1207.
33 M. S. Martín-González, A. L. Prieto, R. Gronsky, T. Sands and A. M. Stacy, *J. Electrochem. Soc.*, 2002, **149**, C546.
34 M. S. Martín-González, G. J. Snyder, A. L. Prieto, R. Gronsky, T. Sands and A. M. Stacy, *Nano. Lett.*, 2003, **3**, 973.
35 F. A. Kröger, *J. Electrochem. Soc.*, 1978, **125**, 2028.
36 E. Koukharenko, X. Li, I. S. Nandhakumar, M. J. Tudor, S. P. Beeby, B. Schiedt, C. Trautmann and N. M. White, *IEE Electron. Lett.*, 2008, **44**, 500.
37 M. Skupinski, M. Toulemonde, M. Lindeberg and K. Hjort, *Nucl. Instrum. Methods Phys. Res., Sect. B*, 2005, **240**, 681.
38 J. P. Heremans, C. M. Thrush, Y. M. Lin, S. B. Cronin and M. S. Dresselhaus, *Phys. Rev. B*, 2001, **63**, 085406.
39 K. Seeger, *Semiconductor Physics*, Spinger-Verlag, Berlin, 3rd edn, 1985.
40 J. P. Heremans, C. M. Thrush, D. T. Morelli and M. Wu, *Phys. Rev. Lett.*, 2002, **88**, 216801.

 This journal is © the Owner Societies 2009